AGU PUBLICATIONS

Water Resources Research

TECHNICAL REPORTS: METHODS

10.1002/2016WR019368

Key Points:
- Probabilistic inter-particle mass transfer is derived
- Upon mass transfer, reactions take place on particles
- No limit to the complexity of on-particle reactions

Correspondence to:
D. A. Benson,
dbenson@mines.edu

Citation:
Benson, D. A., and D. Bolster (2016), Arbitrarily complex chemical reactions on particles, *Water Resour. Res.*, *52*, doi:10.1002/2016WR019368.

Received 15 JUN 2016
Accepted 28 OCT 2016
Accepted article online 3 NOV 2016

Arbitrarily complex chemical reactions on particles

David A. Benson[1] and Diogo Bolster[2]

[1]Hydrologic Science and Engineering, Colorado School of Mines, Golden, Colorado, USA, [2]Department of Civil and Environmental Engineering and Earth Sciences, University of Notre Dame, Notre Dame, Indiana, USA

Abstract Previous particle-tracking (PT) algorithms for chemical reaction conceptualize each particle being composed of one species. Reactions occur by either complete or partial birth/death processes between interacting particles. Here we extend the method by placing any number of chemical species on each particle. The particle/particle interaction is limited to mass exchange. After exchange, reactions of any sort are carried out independently on each particle. The novel components of the algorithms are verified against analytic solutions where possible.

1. Introduction

The random-walk particle-tracking (PT) method is well-established for simulating conservative and first-order reactive transport problems in hydrologic [*Henri and Fernàndez-Garcia*, 2014], oceanic [*Velo-Suárez et al*., 2010; *Lynch et al*., 2015], atmospheric [*Thomson* 1987; *Weil et al*., 2004; *Lin et al*., 2013; *Lauritzen et al*., 2001], and other geophysical settings [*Samelson and Wiggins*, 2006]. The method is well-suited to highly variable velocity fields because it does not suffer from numerical dispersion in the simulation of advection. When moving to higher-order reactions, the particle masses are classically mapped back to grids in a mixed Eulerian/Lagrangian (or semi-Lagrangian) scheme [e.g., *Tompson and Dougherty*, 1992]. Recent work has extended these methods to purely Lagrangian physically based bimolecular reactions [*Benson and Meerschaert* 2008], including sequences of elementary-step reactions that build more complex reactions such as Michaelis-Menten-type kinetics [*Ding and Benson* 2015]. The original algorithm was developed with probabilistic birth/death algorithms that killed and created entire particles. *Bolster et al*. [2016] extended the method by allowing a particle's mass to change based on the amount of reaction it undergoes with nearby particles due to mass transfer. However, each particle was assigned variable mass of only one constituent, and reactions took place *between*, not *on* particles. In this note, we extend the method so that each particle carries mass of any number of constituents, thereby allowing the single-step calculation of arbitrarily complex reactions using standard methods. The new algorithm relies on calculating the correct mass transfer of species between particles, which is based on the previous probabilistic algorithm of *Benson and Meerschaert* [2008]. The new method is shown to reproduce analytic solutions of bimolecular reactions with arbitrary stoichiometry.

2. An Analytic Solution

We will benchmark the new method using the directly solvable reaction

$$pA+qB \underset{k_r}{\overset{k_f}{\rightleftharpoons}} C, \tag{1}$$

where p and q are integer stoichiometric constants. Any rate law can be used in the numerical method, but we will assume that (1) is an elementary step reaction so that there are well-mixed thermodynamic rate coefficients for the forward and reverse reactions k_f and k_r. Without loss of generality we will assume that the activity coefficients are unity so the rate laws can be written in terms of concentrations (denoted by square brackets [ ]):

$$\frac{d[A]}{dt}=\frac{p}{q}\frac{d[B]}{dt}=-k_f[A]^p[B]^q+pk_r[C] \tag{2}$$

$$\frac{d[C]}{dt} = \frac{1}{p} k_f [A]^p [B]^q - k_r [C]. \tag{3}$$

For an analytic solution, against which the numerical approximations can be gauged, assume that the reaction is irreversible ($k_r = 0$), and that the initial concentrations denoted $[A](t=0) \equiv [A]_0$ occur in the ratio $q[A]_0 = p[B]_0$, then the stoichiometry guarantees that $q[A](t) = p[B](t)$. Now (2) is equivalently

$$\frac{d[A]}{dt} = -k_f [A]^p \left(\frac{q}{p}[A]\right)^q = -k_f \left(\frac{q}{p}\right)^q [A]^{p+q}, \tag{4}$$

with solution to the IVP $[A](t=0) = [A]_0$

$$[A]^{1-p-q} = k_f (p+q-1) \left(\frac{q}{p}\right)^q t + [A]_0^{1-p-q}. \tag{5}$$

Converting to dimensionless concentration ($[A]/[A]_0$):

$$[A]/[A]_0 = \left(1 + k_f (p+q-1) \left(\frac{q}{p}\right)^q [A]_0^{p+q-1} t\right)^{1/(1-p-q)}. \tag{6}$$

Our numerical solutions will be compared to this well-mixed solution.

3. Reactions on Particles

To perform reactions on particles, there are several conceptual paths. First, one may consider each particle wholly composed of a unit mass of a single constituent. This is the basis of the algorithms by *Gillespie* [1977] and *Benson and Meerschaert* [2008]. The present approach assumes that a particle can carry masses of many constituents and that the masses on a single particle experience perfect mixing, i.e., the rate laws pertaining to a well-mixed system apply at the particle level. Then particles must exchange mass with each other in order to simulate larger-scale mixing. This may be handled in a probabilistic manner consistent with *Benson and Meerschaert* [2008]. In this framework, particles have some probability of co-location. Two co-located particles will be well-mixed and any differences in masses of constituents will be equalized. For example, a particle with masses of constituents *A* and *B* of 0.5 and 0.5 colliding with a particle with masses of *A* and *B* of 0.1 and 0.9 will give both particles *A* and *B* masses of 0.3 and 0.7. Thus we may view the mass exchange as a reaction in the sense of *Bolster et al*. [2016]: in this case the reaction is mixing characterized by mass transfer and equalization between the particles. Any particle has some probability of co-locating with nearby particles, so following *Bolster et al*. [2016], the mass transfer between any particles is weighted by the probability of co-location. Nearby particles exchange more mass in any time period because their co-location probability is greater. The equation for change of mass between two particles labeled by superscripts 1 and 2, for every species *j* on each particle, follows

$$dm_j^1 = \frac{1}{2}(m_j^2 - m_j^1) v(s) ds, \tag{7}$$

where $v(s)$ is the particle co-location probability density given particle separation distance *s*. For diffusive systems with species-dependent diffusion coefficients $D_j \geq 0$, the density is the convolution of the location densities of the species *j* held in the two particles over the time step *dt*. In d-dimensions, $v(s) = [\exp(-|s|^2/(4dt(D_j^1 + D_j^2))]/(4\pi dt(D_j^1 + D_j^2))^{d/2}$, although this can be generalized to other mass transfer mechanisms [e.g., *Bolster et al*., 2012]. We can also define solid phase particles; a species in a solid-phase particle has $D = 0$. The mixing by mass transfer is weighted by each particle pair's proximity, because $v(s)ds$ is the probability of co-location for that pair (schematically represented in Figure 1). Equation (7) recognizes that at some particle support volume *ds*, full mixing would occur: if two particles have unit probability of colocation, then the masses of species are shared equally among them. (Theoretically this can only happen for two motionless coincident particles, then $v(s=0) = \delta(s)$ and $v(s=0)ds = 1$). In practice, only partial mixing is seen between any two particles, and the mixing is exactly dictated by the probability of diffusional collision. It is important to note that, numerically, particles need not actually collide. Equation (7) accounts for probabilistic mass transfer among all particles, even if $v(s)ds$ becomes vanishingly small outside of some typical diffusion radius. Intuitively, the *d*-dimensional size *ds* is related to particle spacing: each particle is a

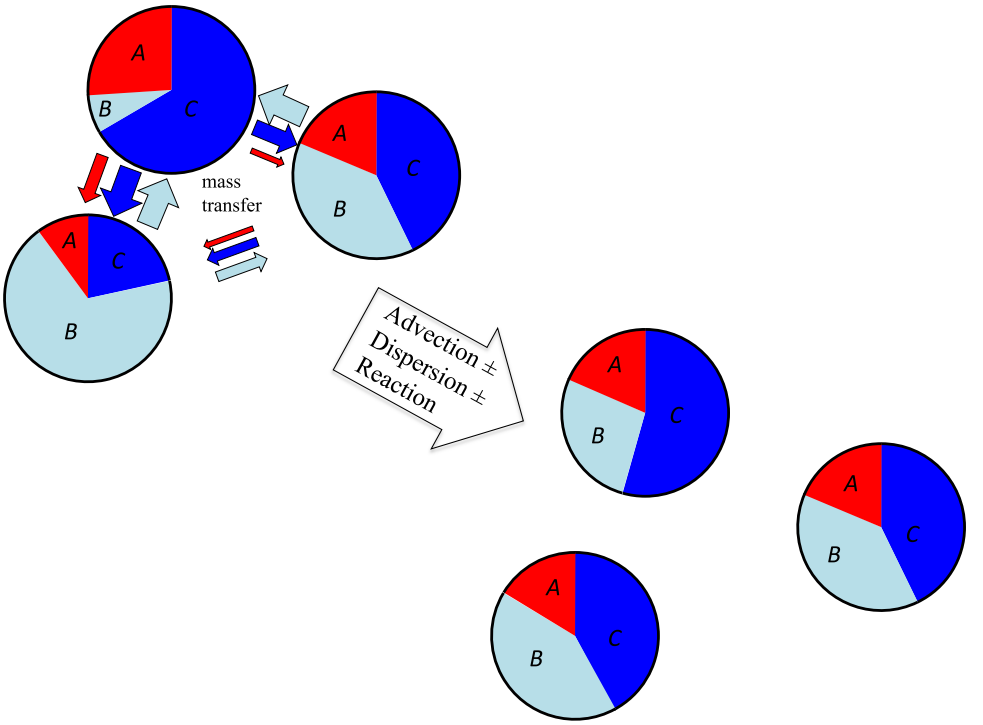

Figure 1. Schematic representation of mass transfer and particle motion operations split in a time step. The mass transfer is proportional to mass difference between particles and the probability of colocation, which decreases with separation distance. Colored arrow size is representative of transfers according to equation (7).

Dirac delta function but the mass is spread over some inter-particle distance in order to approximate a smooth concentration field, i.e., each particle has an average support volume equal to the average spacing. A more rigorous derivation of *ds* is given in Appendix A.

Particles may move under the forces of advection, hydrodynamic dispersion, and molecular diffusion [*Labolle et al*., 1996; *Salamon et al*., 2006]. The mass exchange in (7) is applied to all particle pairs for which the probability is nonnegligible (Figure 1). After mass exchange operations, there may be new ratios of species masses on a particle, so the laws of reaction in any form can be applied, including the effects of ionic strength on activity coefficients, etc. Without loss of generality we demonstrate with a simple rate law (2) with $k_r = 0$.

It is somewhat artificial to distinguish between particle mass and particle concentration. The initial concentration of A in a simulation is distributed among N_A particles according to $m_{A0} = [A]_0 L/N_A$. Each particle represents concentration $[A]_0$ over a volume L/N_A. As the mass changes by mass transfer, the concentration of A on particle i is just $[A]^i = [A]_0 m_A^i / m_{A0}$. The same may be written for any species. With a relationship between mass and concentration for each species on each particle, it is easy to formulate any concentration-based reactions after some mass exchange. For example, the forward reaction in (2) has a first-order numerical implementation

$$d[A]^i = -k_f\, dt\, ([A]^i)^p ([B]^i)^q \tag{8}$$

$$dm_A^i \frac{[A]_0}{m_{A0}} = -k_f\, dt \left(\frac{[A]_0 m_A^i}{m_{A0}}\right)^p \left(\frac{[B]_0 m_B^i}{m_{B0}}\right)^q \tag{9}$$

$$dm_A^i = -k_f\, dt\, \frac{m_{A0}}{[A]_0} \left(\frac{[A]_0 m_A^i}{m_{A0}}\right)^p \left(\frac{[B]_0 m_B^i}{m_{B0}}\right)^q \tag{10}$$

$$dm_A^i = -(m_A^i)^p (m_B^i)^q\, k_f\, dt \left(\frac{[A]_0}{m_{A0}}\right)^{p-1} \left(\frac{[B]_0}{m_{B0}}\right)^q. \tag{11}$$

All terms to the right of $(m_B^i)^q$ are constants defined by time step size, reaction kinetics, stoichiometry, and initial conditions. Furthermore, very fast reactions—which on the face of equation (11) might yield mass changes that exceed the amount of mass on a particle—can be easily handled by determining the limiting reactant on a particle. First, the potential change in all species masses is calculated and compared to the amount on a particle. Then the limiting, or minimum mass, governs the extent of the reaction. In the two-reactant case there are two conditions, which stoichiometry reduces to one:

$$\begin{aligned} -dm_A^i &= \min\left(-dm_A^i, m_A^i\right) \text{ and } -dm_B^i = \frac{-q}{p} dm_A^i = \min\left(\frac{-q}{p} dm_A^i, m_B^i\right), \\ -dm_A^i &= \min\left[\min\left(-dm_A^i, m_A^i\right), \min\left(-dm_A^i, \frac{p}{q} m_B^i\right)\right] \\ -dm_A^i &= \min\left(-dm_A^i, m_A^i, \frac{p}{q} m_B^i\right) \end{aligned} \tag{12}$$

4. Verification

There are several aspects to the reactions-on-particles algorithm that are novel and must be verified. As far as we know, the probabilistic mass transfer algorithm is new, but contains some verifiable boundary and initial value problems. For example, if a sharp interface is created (wherein all particles to the right are 100% *A* and all particles to the left are initially 100% *B*), then mass transfer should follow the purely diffusive propagation of the *A* and *B* masses across the domain, even though the particles are not moving at all. Only the probabilities of collision are calculated and masses transferred according to this probability using (7). We recognize that this is not the most efficient manner to simulate diffusive mass transfer; however, it is critical to the reactions-on-particles algorithm. A simulation was created in this way with $N=10^3$ uniformly random particle positions in a periodic domain $[0, L]$ with $L = 1$ (Figure 2). The diffusion coefficient is $D=10^{-5}$ with time steps $\Delta t=1$ for a total time of 100 and the "size" of a particle (i.e., the perfect mixing length) is set to

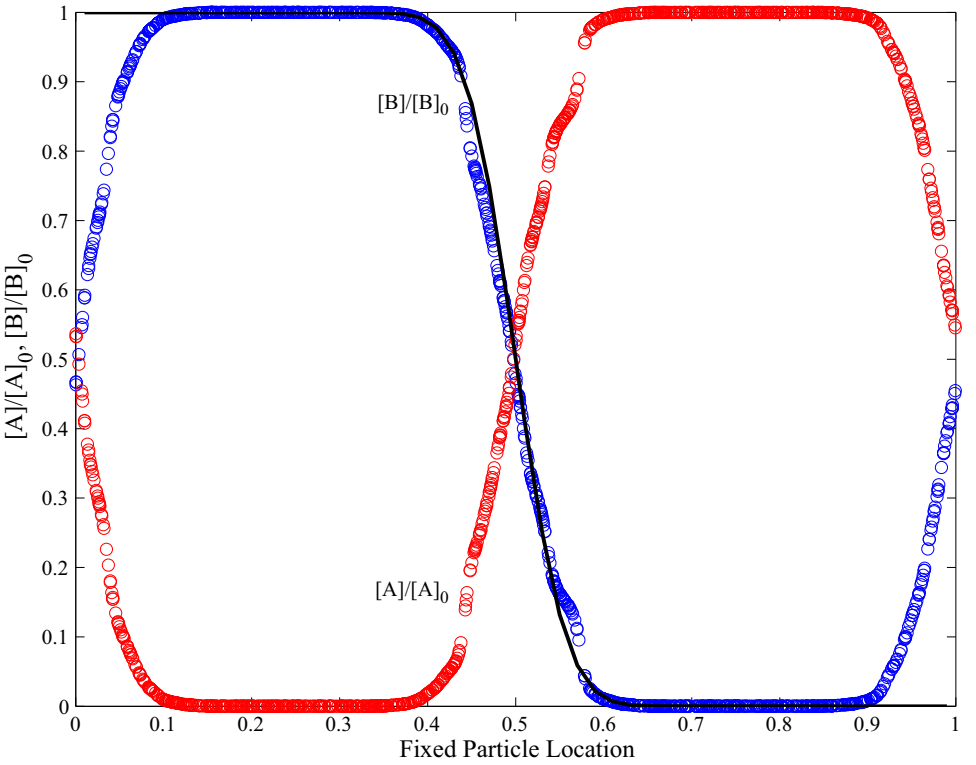

Figure 2. Diffusion on a periodic 1-*d* domain via probabilistic mass transfer among 1000 fixed particles in space. Total time = 100 and $D=10^{-5}$. Each particle has *A* (red) and *B* (blue) mass, with initial condition on each particle $A(0.5 \le x \le 1)=B(0 \le x \le 0.5)=1$ and zero otherwise. Black line is the analytic solution for the *B* diffusion profile in the center of the domain.

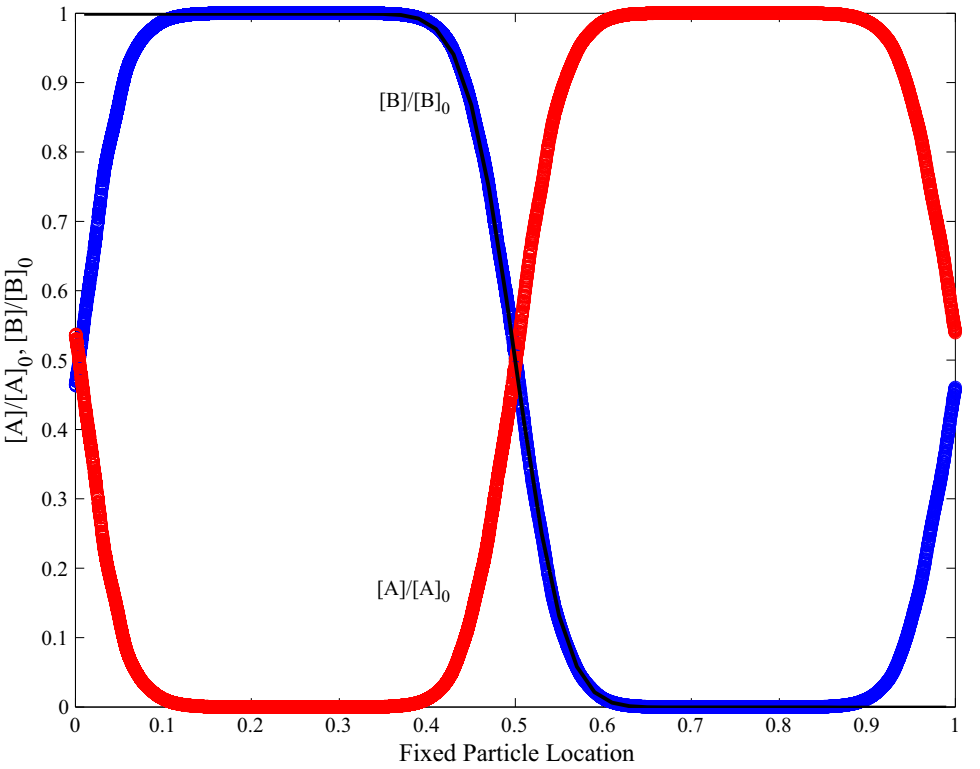

Figure 3. Diffusion on a periodic 1-*d* domain via probabilistic mass transfer among 10,000 fixed particles in space. Total time = 100 and $D=10^{-5}$. Each particle has *A* (red) and *B* (blue) mass, with initial condition on each particle $A(0.5 \leq x \leq 1)=B(0 \leq x \leq 0.5)=1$ and zero otherwise. Black line is the analytic solution for the *B* diffusion profile in the center of the domain.

$ds=L/N$. With stationary particles following rule (7), the analytic diffusion profile is followed, although in areas of larger random particle spacing, the mass transfer is more limited (as expected). Increasing the number of particles to $N=10^4$ promotes a profile closer to the analytic solution across the entire domain (Figure 3).

Next we verify the classic irreversible reaction $A+B \rightarrow C$. Under well-mixed conditions, the solution following (6) decays at long times with t^{-1}. Previous PT simulations of this reaction follow the well-mixed solution until self-segregation of the reactants into "islands" slows the reaction rate to $t^{-1/4}$. The time at which the simulations make this transition depends on the particle Damköhler number $kA_0/(D/ds^2)$, where *ds* is the average particle spacing *L*/*N*. In those previous simulations, diffusion was modeled by random motions of the particles, and each particle only carried mass of one species [*Paster et al*., 2014; *Bolster et al*., 2012, 2016]. Here we simulate diffusive mass transfer between fixed particles with (7) and subsequent reaction with (2). We also verified the method with more complex reactions with $p \neq q$ (here we only show $p=1$, $q=3$). With a large $D=10^{-2}$, the simulated reactions remain well-mixed over the duration of the simulations $t=100$ in a 1-*d* domain $L=1$ (Figure 4) and match the analytic solutions.

4.1. Combined Transport and Reaction

The previous verification simulations transferred mass without moving particles. Most often, particles in simulations are put in motion to simulate advection and mechanical dispersion. In this section, we verify that the diffusive flux previously shown is additive to any mechanical dispersion. In a subsequent section (showing interaction with solids) we will also add advection and limit mass transfer to a much smaller molecular diffusion coefficient. In 1-*d* we generated simulations in which half of the diffusion in each time step is done by random walks [e.g., *Labolle et al*., 1996] followed by another half by mass transfer among (temporarily) stationary particles. These simulations are compared to those in which diffusion and reaction are always carried out on stationary particles. The effects of diffusion magnitude are most easily seen in the time at which the PT solutions diverge from the well-mixed solution [*Paster et al*., 2014]. We choose $p=q=1$,

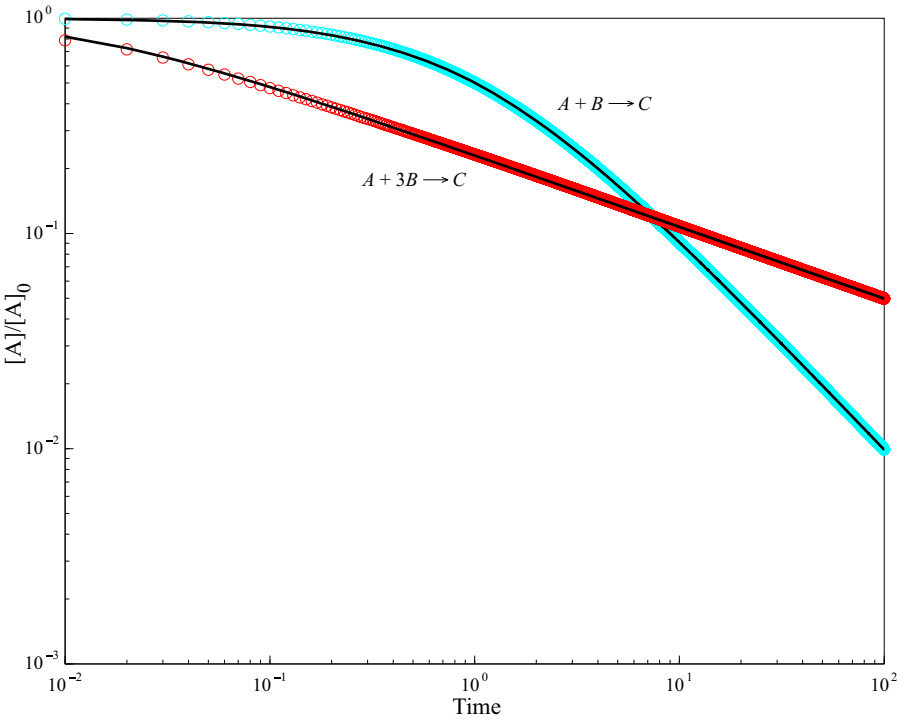

Figure 4. Simulated domain-average $[A](t)/[A]_0$ due to diffusive mass transfer of A and B and reaction according to (1) on a periodic 1-d domain among 1,000 fixed particles in space. Total time = 100, $D=10^{-2}$, $k_f = 1$, $[A]_0=1$, and $[B]_0=q[A]_0$. Simulations are for $p=1$ and $q = 1$ and 3 (blue and red symbols, respectively). Solid curves are for the corresponding analytic solutions (6).

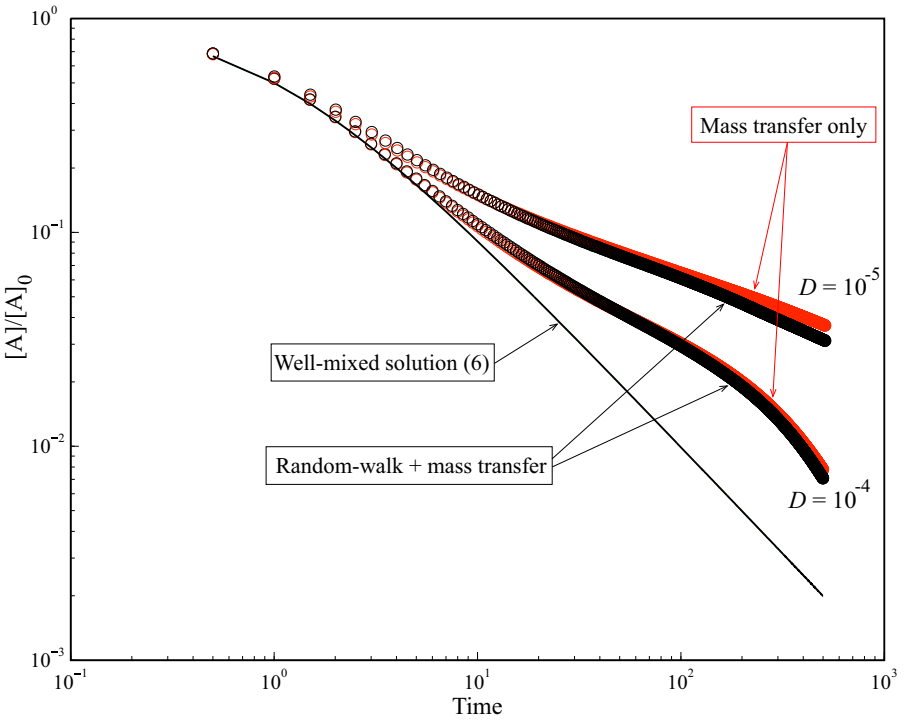

Figure 5. Ensemble means of 20 simulations with reaction and diffusion either by mass transfer on fixed particles (red symbols) or half by random motion and half by mass transfer (black symbols). Two different diffusion coefficients $D=10^{-4}$ and 10^{-5} are used, so the Damköhler numbers are approximately 10 and 100, respectively. The diffusion is small enough that these solutions slow relative to the well-mixed solution (6), shown by a solid black curve. The simulated reaction is $A+B \rightarrow C$.

$k_f = 1$, $dt = 0.5$, and $D = 10^{-4}$ and 10^{-5}. For the larger diffusion coefficient, the two methods for simulating diffusion and reaction are essentially identical (Figure 5). Differences are seen for the smaller D because a smaller effective influence of particles causes a small number of mass transfer "gaps" that can be seen in Figure 2. In our initial condition, 1000 particles were uniformly randomly distributed on $x = [0, 1]$ which means that there will be some larger random gaps. We can equivalently randomize the initial condition by deterministically placing the particles with exact spacing $\Delta x = 1/1000$ and randomize which of the particles begin with either 100% A or 100% B. Such a simulation was created and matches the half RW/half mass transfer simulation with $D = 10^{-5}$ much more closely (not shown here for brevity).

4.2. Instantaneous Reactions

Simulating very fast reactions was a problem for the original particle-killing reaction algorithm [see *Ding et al.*, 2012], because the probability of reaction was linear with $k_f \Delta t$. Equation (12) allows any forward rate, so we may compare our solutions to the analytic solution for instantaneous reactions [*Gramling et al.*, 2002]. For reactions following $A + B \rightarrow C$ with the initial sharp interface initial condition and diffusion as in Figure 2, the concentration of product follows an analytic solution $C(x,t) \approx \sum_i 0.5 \operatorname{erfc}(|x - x_i|/\sqrt{4Dt})$, where x_i is the position of the interfaces. Using $k_f = 10^9$, $[A]_0 = [B]_0 = 1$, $D = 0.001$, and $N = 10^4$, the particle Damköhler number is 10^4. Both the mass transfer (with fixed but randomly placed) particles and the half random walk/half mass transfer methods show excellent agreement with the analytic solution at $t = 2$ (Figures 6 and 7, respectively). The agreement further validates that the different simulated mechanisms for diffusion are additive.

4.3. Interaction With a Solid Phase

In principle any number of heterogeneous reactions can potentially be simulated with this particle method. Without loss of generality, here we simulate instantaneous and reversible conversion of aqueous concentration to solid phase concentration. This idealization of reaction gives the familiar retardation factor [*Lapidus and Amundson*, 1952; *Reynolds et al.*, 1982], which admits analytic solutions. We add advection and

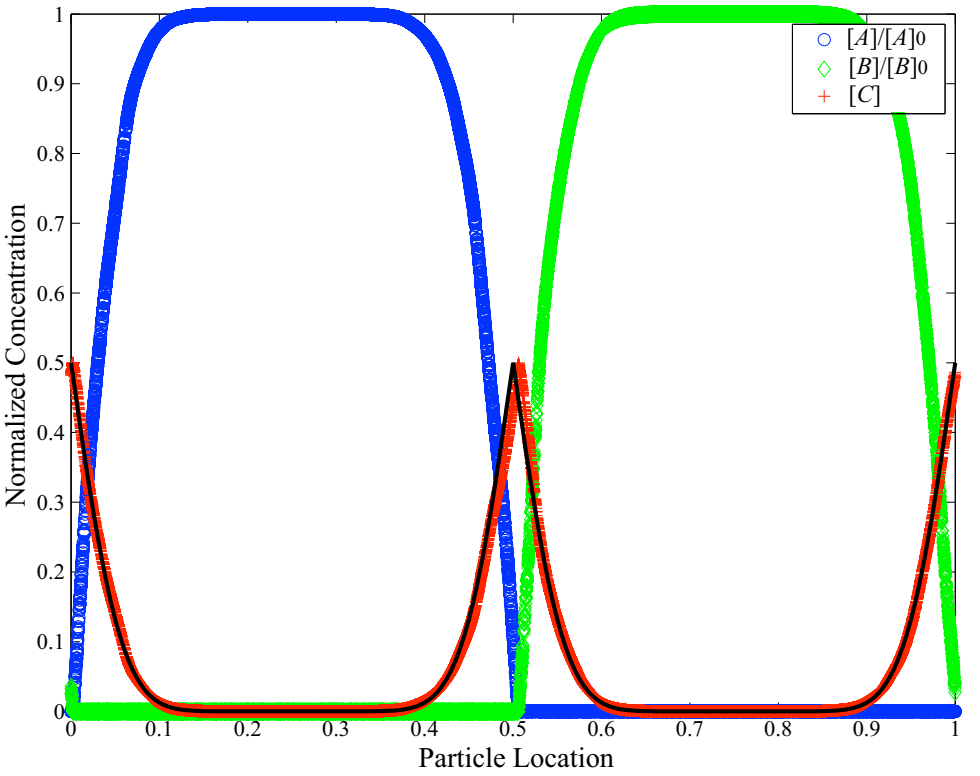

Figure 6. Single realization of fast (essentially instantaneous) reaction resulting from initially sharp interfaces between A and B. Periodic domain had initial interfaces at $x = 0 = 1$ and $x = 0.5$. Diffusion is simulated purely by mass transfer among fixed-position particles that are uniformly randomly distributed on $x = [0, 1]$. Black line is analytic solution.

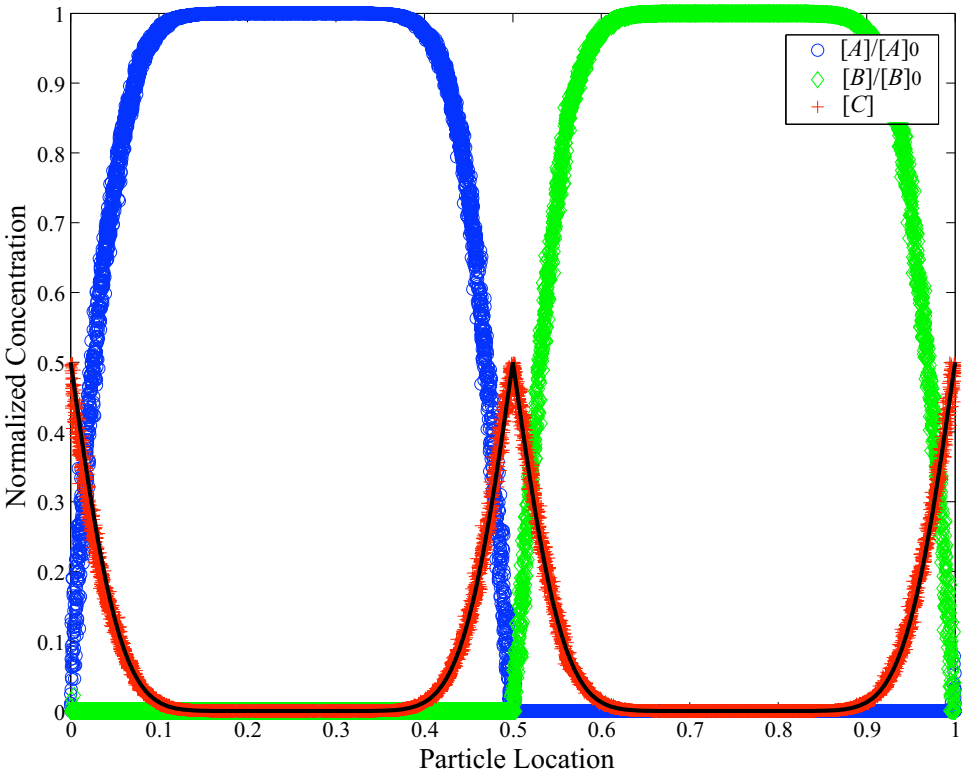

Figure 7. Single realization of fast (essentially instantaneous) reaction resulting from initially sharp interface between *A* and *B*. Periodic domain had initial interfaces at $x=0=1$ and $x=0.5$. Diffusion is simulated half by random walks and half by mass transfer among stationary particles between motions. Black line is analytic solution.

dispersion as hydraulic processes that act on mobile particles and diffusion, which allows mass transfer between mobile/mobile and mobile/immobile particles. The algorithm for each interaction remains the same except that the diffusion coefficient for immobile particles is zero. All things held the same, a mobile particle needs to be closer to an immobile particle to exchange the same amount of mass.

For these advection-dispersion-sorption simulations, we use unit porosity and unit bulk density, so that the familiar retardation factor is the ratio of total mass to mobile mass, i.e., $R=1+K_d^j$, where K_d is the distribution coefficient for species *j*. For these instantaneous reactions, K_d is the ratio of sorbed to mobile mass.

The instantaneous mobile/immobile mass transfer can be simulated using equation (7) with an unequal equilibrium. As opposed to mobile/mobile equilibrium, the mass is not split half-and-half. When a mobile particle (1) is compared to an immobile particle (2), the mass transfer follows

$$dm_j^1 = \frac{1}{1+K_d^j}\left(m_j^2 - K_d^j m_j^1\right)v(s)ds. \tag{13}$$

Simulations were run by randomly placing 4000 mobile and 4000 immobile particles in a 1-D periodic domain $x=[0,1]$. At time $t=0$, one mobile and one immobile particle are placed at $x=0.2$ with total masses of species *A* and $B=1.0$, split between mobile and immobile phases according to the K_d^j. After $t=0$, all particles may carry any masses of species *A* and *B*. Mobile particles are moved according to the velocity and hydrodynamic dispersion parameters $v=1$ and $D_{hyd}=4\times10^{-3}$. Diffusive mass transfer in equation (7) and equation (13) use a mobile-phase diffusion coefficient of $D_m=4\times10^{-5}$. It is important to note that the operator-splitting of the idealized process of instantaneous sorption makes this simulation accurate to $\mathcal{O}(\Delta t)$. Physically, particles should not move too long in the mobile phase without sorptive mass transfer.

Distribution coefficients were chosen as $K_d^A=0$ and $K_d^B=2.5$, for retardation coefficients of 1 and 3.5. Simulations for a range of $\Delta t \in \{0.01, 0.001, 0.0001\}$ over a total time of $t=0.5$ show that the largest time step

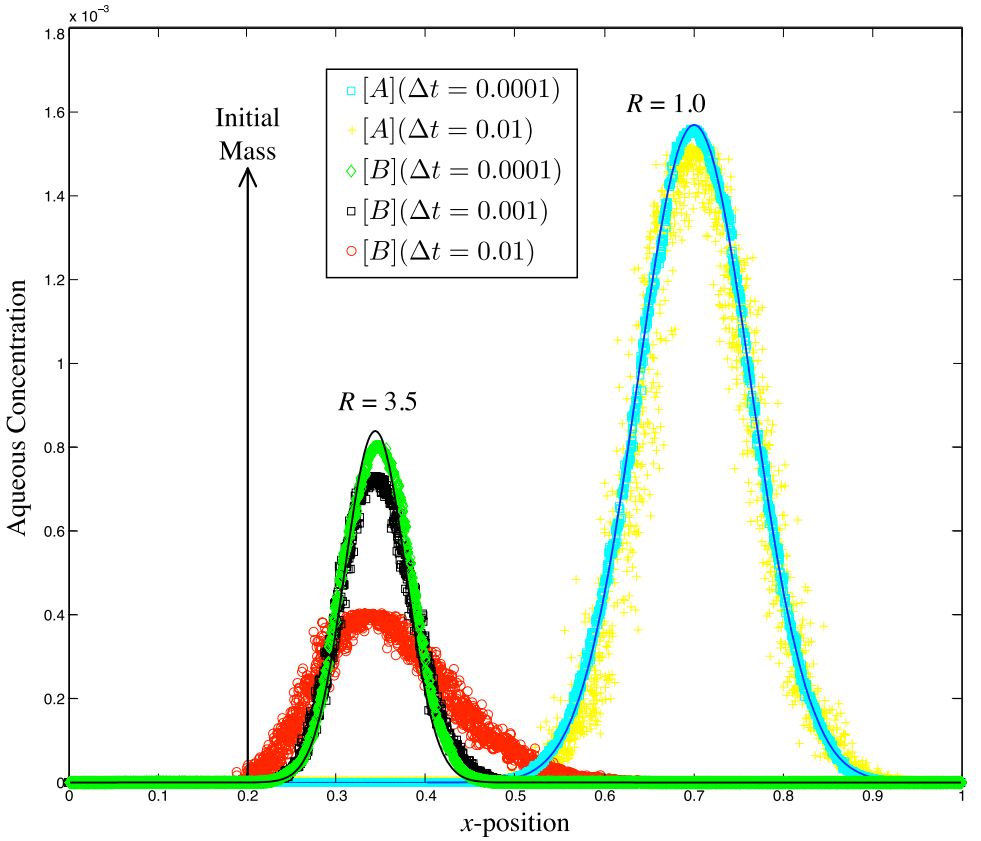

Figure 8. Mobile concentrations (symbols) from simulations of particles carrying species *A* and *B* that interact with immobile particles. Distribution coefficients are $K_d^A = 0$ and $K_d^B = 2.5$ for retardations coefficients of 1 and 3.5, respectively. Time step sizes from 0.01 to 0.0001 are shown. Analytic solutions shown by continuous curves.

incurs significant error for $R = 3.5$ (Figure 8). The first moments of all simulated plumes are fairly accurate (all within several percent of the analytic solutions). The centered second moments—the so-called plume variance—show more error that grows with time step size. For the largest time step used here, the plume variance is about 4.5 times larger than the analytic solution over the entire simulation (Figure 9). The medium time step gives excess variance by a factor of 1.4 and the smallest time step essentially no difference on average (Figure 9). Clearly the split mobile/immobile algorithm engenders a numerical dispersion that appears to be $\mathcal{O}(\Delta t)$ and a function of sorption strength. Note also that larger time steps give larger variability of the concentration at any place, even though plume moments are correctly simulated in the case of $R = 1$ (Figure 9).

5. Remarks

Advection, dispersion, diffusive mass transfer, and arbitrarily complex reactions may all be performed on, and between, particles. The key here is a new algorithm for diffusive mass transfer between particles according to proximity and probability of co-location. After mass transfer of all species between mobile and immobile phases is performed, the reactions can be calculated using standard methods based on concentrations using the proportionality constant relating species masses to concentrations on each particle. The potential benefits of particle-tracking methods have been discussed elsewhere in the context of simple bimolecular reactions: the particles do not have a Courant number criterion for stability, and the number of particles is very often going to be smaller than the number of cells in a typical grid-based simulation, so that the number of numerical geochemical calculations is similarly smaller.

The method currently splits the 1) hydraulic motion, 2) mass transfer, and 3) reaction operations. We have not yet investigated the absolute magnitudes of error introduced by the operator splitting. Ongoing work seeks to find single (unsplit) Langevin equations for motions and reaction [e.g., *Benitez et al.*, 2016], but

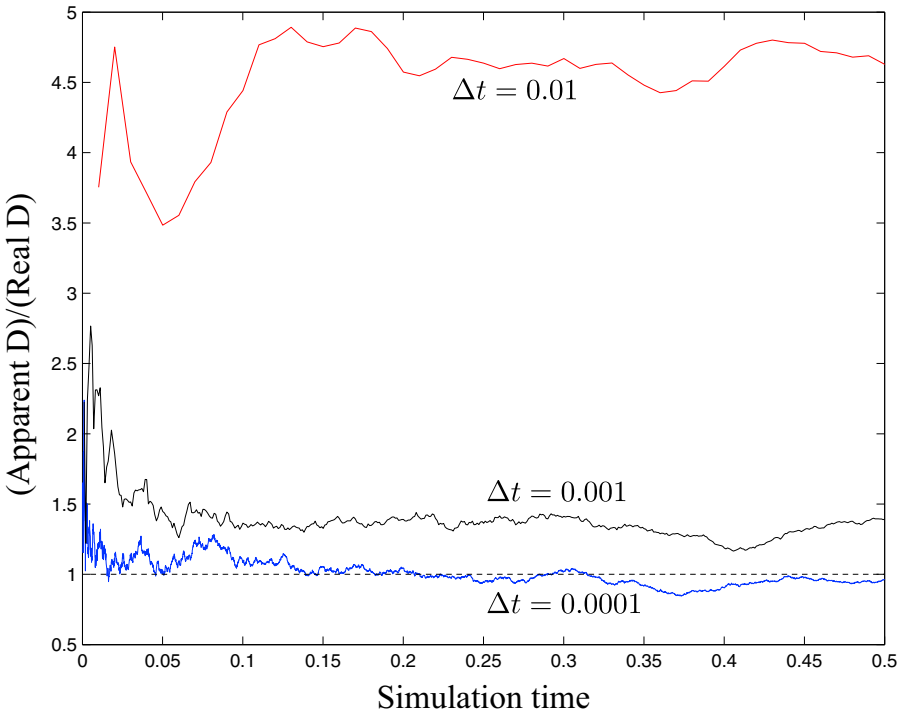

Figure 9. Ratio of simulated to analytic plume variance for the $R = 3.5$ plumes for timestep sizes (top) 0.01, (middle) 0.001, and (bottom) 0.0001.

these efforts are not fully realized for complex reactions that may be found in a typical hydrologic system such as an aquifer. In our example using instantaneous sorption, the error manifests in different ways (plume variance versus variance of $C[x, t]$), based on sorption strength. Our example is potentially the strictest test: theoretically, the idealized instantaneous reactions are based on an infinite number of mass transfers between aqueous and solid phases in any time interval. Rate-limited sorption and water-rock interactions have a set number of transitions dictated by the reaction rates.

Our method is verified using bimolecular reactions with arbitrary stoichiometry, but the method is clearly not restricted in the chemistry that is allowed. For example, PHREEQC [*Parkhurst and Appelo*, 2013], CRUNCHFLOW [*Steefel*, 2009], or similar codes can be applied to chemistry on the particles in the same manner as grid-based simulators. These types of reactions, and the absolute errors, will be investigated in future studies.

Appendix A: Heuristic Derivation of *ds*

Imagine a simplified system in which (for the sake of calculations only), all N particles are spaced evenly in domain Ω with spacing $\Delta x = \Omega/N$. A delta function initial condition evolves over some t to a Gaussian Green function. Consider the decrease in concentration over time step dt at the peak (call this point $x = 0$), which should evolve as

$$dm = \frac{1}{\sqrt{4\pi D(t+dt)}} - \frac{1}{\sqrt{4\pi Dt}}. \tag{A1}$$

For the simplified system we can directly calculate the change in mass at the "peak" particle using equation (7). Each particle is located an integer multiple of Δx from the peak, so $x_n = n\Omega/N$. The sum is over half of the particles due to symmetry:

$$dm = 2\sum_{n=1}^{N/2} \frac{1}{2}\left(\frac{1}{\sqrt{4\pi Dt}}\exp\left(-(n\Omega/N)^2/4Dt\right) - \frac{1}{\sqrt{4\pi Dt}}\right)\times \frac{1}{\sqrt{8\pi Ddt}}\exp\left(-(n\Omega/N)^2/8Ddt\right)\times ds \tag{A2}$$

Equating these expressions for dm and solving (numerically) for ds gives $ds = \Omega/N$, for any parameter values N, Ω, D, t, and dt tested. Experimentally, this value also works for randomly placed particles.

Acknowledgements
This work was supported by the National Science Foundation (grants EAR-1351625 and EAR-1417264). All equations and data required to reproduce this work are listed in the text and figures.

References

Benitez, F., C. Duclut, H. Chaté, B. Delamotte, I. Dornic, and M. A. Muñoz (2016), Langevin equations for reaction-diffusion processes, *Phys. Rev. Lett.*, *117*, 100,601, doi:10.1103/PhysRevLett.117.100601.

Benson, D. A., and M. M. Meerschaert (2008), Simulation of chemical reaction via particle tracking: Diffusion-limited versus thermodynamic rate-limited regimes, *Water Resour. Res.*, *44*, W12201, doi:10.1029/2008WR007111.

Bolster, D., P. de Anna, D. A. Benson, and A. M. Tartakovsky (2012), Incomplete mixing and reactions with fractional dispersion, *Adv. Water Resour.*, *37*, 86–93, doi:10.1016/j.advwatres.2011.11.005.

Bolster, D., A. Paster, and D. A. Benson (2016), A particle number conserving Lagrangian method for mixing-driven reactive transport, *Water Resour. Res.*, *52*, 1518–1527, doi:10.1002/2015WR018310.

Ding, D., and D. A. Benson (2015), Simulating biodegradation under mixing-limited conditions using Michaelis–Menten (Monod) kinetic expressions in a particle tracking model, *Adv. Water Resour.*, *76*, 109–119, doi:10.1016/j.advwatres.2014.12.007.

Ding, D., D. Benson, A. Paster, and D. Bolster (2012), Modeling bimolecular reactions and transport in porous media via particle tracking, *Adv. Water Resour.*, *53*, 56–65, doi:10.1016/j.advwatres.2012.11.001.

Gillespie, D. T. (1977), Exact stochastic simulation of coupled chemical reactions, *J. Phys. Chem.*, *81*(25), 2340–2361.

Gramling, C., C. Harvey, and L. Meigs (2002), Reactive transport in porous media: A comparison of model prediction with laboratory visualization, *Environ. Sci. Technol.*, *36*(11), 2508–2514, doi:10.1021/es0157144.

Henri, C. V., and D. Fernàndez-Garcia (2014), Toward efficiency in heterogeneous multispecies reactive transport modeling: A particle-tracking solution for first-order network reactions, *Water Resour. Res.*, *50*, 7206–7230, doi:10.1002/2013WR014956.

Labolle, E. M., G. E. Fogg, and A. F. B. Tompson (1996), Random-walk simulation of transport in heterogeneous porous media: Local mass-conservation problem and implementation methods, *Water Resour. Res.*, *32*(3), 583–593.

Lapidus, L., and N. R. Amundson (1952), Mathematics of adsorption in beds. VI. the effect of longitudinal diffusion in ion exchange and chromatographic columns, *J. Phys. Chem.*, *56*, 984–988.

Lauritzen, P. H., C. Jablonowski, M. A. Taylor, and R. D. Nair (Eds.) (2001), *Numerical Techniques for Global Atmospheric Models, Lecture Notes Comput. Sci. Eng. 80*, Springer, Berlin.

Lin, J., D. Brunner, C. Gerbig, A. Stohl, A. Luhar, and P. Webley (Eds.) (2013), *Lagrangian Modeling of the Atmosphere, Geophys. Monogr. Ser.*, vol. 200, AGU, Washington, D. C.

Lynch, D. R., D. A. Greenberg, A. Bilgiti, D. J. McGillicuddy Jr., J. Manning, and A. L. Aretxabaleta (2015), *Particles in the Coastal Ocean, Theory and Application*, Cambridge Univ. Press, New York.

Parkhurst, D. L., and C. Appelo (2013), Description of input and examples for PHREEQC version 3–A computer program for speciation, batch-reaction, one-dimensional transport, and inverse geochemical calculations, U.S. Geol. Surv. Tech. Methods, *Book 6, Chap. A43*, 497 pp.

Paster, A., D. Bolster, and D. A. Benson (2014), Connecting the dots: Semi-analytical and random walk numerical solutions of the diffusion–reaction equation with stochastic initial conditions, *J. Comput. Phys.*, *263*, 91–112, doi:10.1016/j.jcp.2014.01.020.

Reynolds, W. D., R. W. Gillham, and J. A. Cherry (1982), Evaluation of distribution coefficients for the prediction of strontium and cesium migration in a uniform sand, *Can. Geotech. J.*, *19*(1), 92–103.

Salamon, P., D. Fernàndez-Garcia, and J. J. Gómez-Hernández (2006), A review and numerical assessment of the random walk particle tracking method, *J. Contam. Hydrol.*, *87*(3–4), 277–305, doi:10.1016/j.jconhyd.2006.05.005.

Samelson, R. M., and S. Wiggins (2006), *Lagrangian Transport in Geophysical Jets and Waves: The Dynamical Systems Approach, Interdisciplinary Appl. Math.*, vol. 31, Springer, New York.

Steefel, C. I. (2009), *CrunchFlow Software for Modeling Multicomponent Reactive Flow and Transport CrunchFlow CRUNCHFLOW, Software for Modeling Multicomponent Reactive Flow and Transport, USER'S MANUAL*, Earth Sci. Div., Lawrence Berkeley Natl. Lab., Berkeley, Calif.

Thomson, D. J. (1987), Criteria for the selection of stochastic models of particle trajectories in turbulent flows, *J. Fluid Mech.*, *180*, 529–556, doi:10.1017/S0022112087001940.

Tompson, A., and D. Dougherty (1992), Particle-grid methods for reacting flows in porous-media with application to Fisher equation, *Appl. Math. Modell.*, *16*(7), 374–383.

Velo-Suárez, L., B. Reguera, S. González-Gil, M. Lunven, P. Lazure, E. Nézan, and P. Gentien (2010), Application of a 3D Lagrangian model to explain the decline of a Dinophysis acuminata bloom in the Bay of Biscay, *J. Mar. Syst.*, *83*(3–4), 242 – 252, doi:10.1016/j.jmarsys.2010.05.011.

Weil, J. C., P. P. Sullivan, and C.-H. Moeng (2004), The use of large-eddy simulations in Lagrangian particle dispersion models, *J. Atmos. Sci.*, *61*(23), 2877–2887, doi:10.1175/JAS-3302.1.